Inhibition of the E3 ligase UBR5 stabilizes TERT and protects vascular organoids from oxidative stress

Haijing Zhao[1,2†], Nian Cao[1†], Qi Liu[2†], Yingyue Zhang[1,2], Rui Jin[4], Huiying Lai[5], Li Zheng[6], Honghong Zhang[1,2], Yue Zhu[1,2], Yuhan Ma[6], Zengao Yang[7], Zhengfeng Wu[1,2], Weini Li[8], Yuqi Liu[1,9,10,11*] , Long Cheng[3,4*] and Yundai Chen[1*]

Abstract

Background Excessive oxidative stress is known to cause endothelial dysfunction and drive cardiovascular diseases (CVD). While telomerase reverse transcriptase (TERT) shows protective effects against oxidative stress in rodents and is associated to human flow-mediated dilation in CVD, its regulatory mechanisms in human vascular systems under pathological oxidative stress require further investigation.

Methods Human induced pluripotent stem cells (hiPSCs) were used to create vascular organoids (VOs). These VOs and human umbilical vein endothelial cells (HUVECs) were subjected to oxidative stress through both hydrogen peroxide (H_2O_2) and oxidized low-density lipoprotein (oxLDL) models. The effects of TERT overexpression by inhibition of the ubiquitin protein ligase E3 component N-recognin 5 (UBR5) on reactive oxygen species (ROS)-induced vascular injury and cellular senescence were assessed using neovascular sprouting assays, senescence-associated β-galactosidase (SA-β-Gal) staining, and senescence-associated secretory phenotype (SASP) assays.

Results ROS significantly impaired VO development and endothelial progenitor cell (EPC) angiogenesis, evidenced by reduced neovascular sprouting and increased senescence markers, including elevated SA-β-Gal activity and SASP-related cytokine levels. Overexpression of TERT counteracted these effects, restoring VO development and EPC function. Immunoprecipitation-mass spectrometry identified UBR5 as a critical TERT regulator, facilitating its degradation. Inhibition of UBR5 stabilized TERT, improving VO angiogenic capacity, and reducing SA-β-Gal activity and SASP cytokine levels.

Conclusions Inhibiting UBR5 stabilizes TERT, which preserves EPC angiogenic capacity, reduces VO impairment, and delays endothelial cell senescence under oxidative stress. These findings highlight the potential of targeting UBR5 to enhance vascular health in oxidative stress-related conditions.

Keywords Vascular organoids, UBR5, TERT, Senescence, Oxidative stress

---

†Haijing Zhao, Nian Cao and Qi Liu have contributed equally to this article.

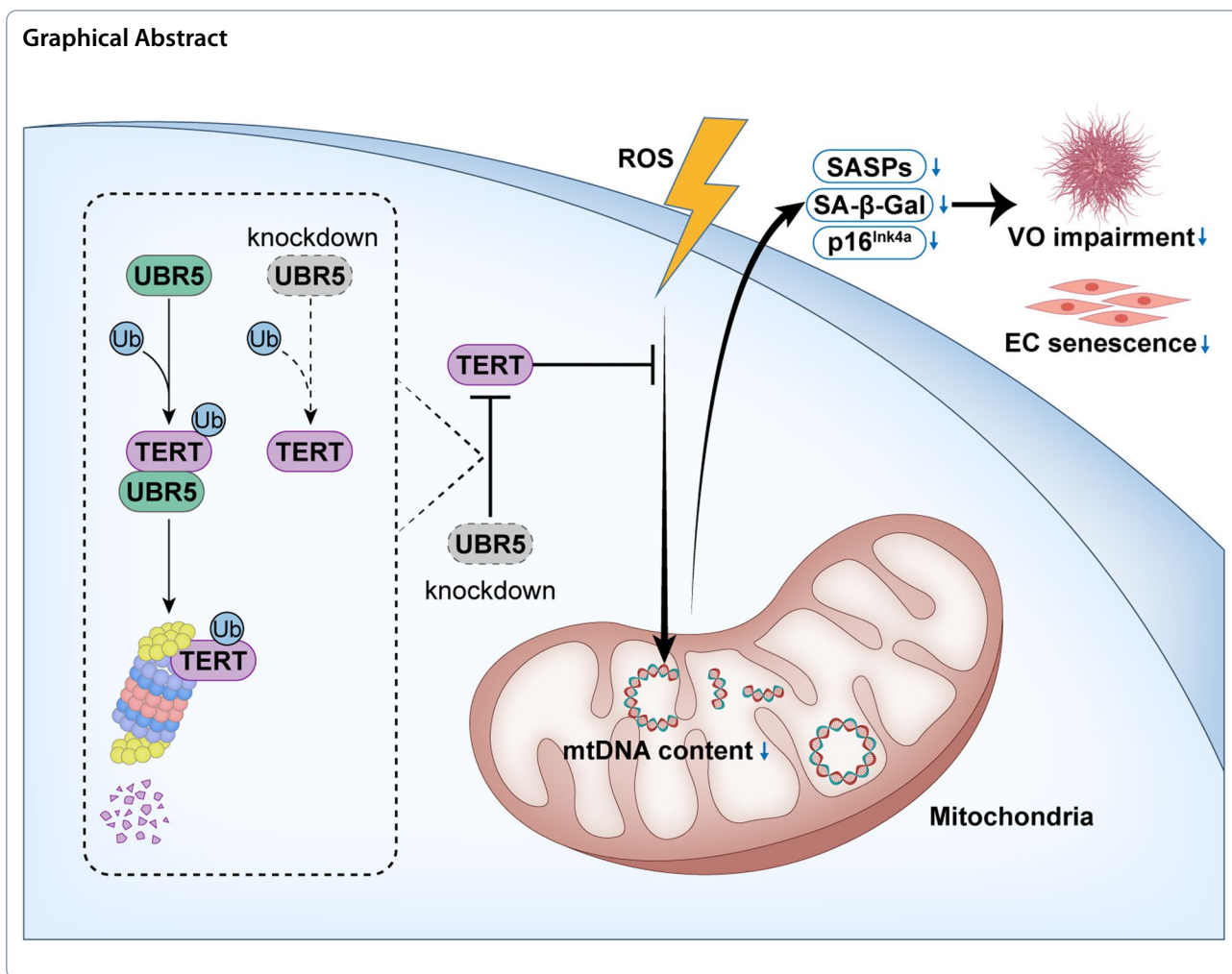*Correspondence:
Yuqi Liu
ametuofo980869@163.com
Long Cheng
biolongcheng@outlook.com
Yundai Chen
cyundai@vip.163.com
Full list of author information is available at the end of the article

Zhao *et al. Journal of Translational Medicine*   (2024) 22:1080

Page 2 of 18

Graphical Abstract

Background

Compelling evidence suggests that elevated levels of reactive oxygen species (ROS) contribute significantly to endothelial dysfunction and various cardiovascular diseases (CVD), including pulmonary arterial hypertension, hypertension, atherosclerosis, and myocardial infarction [1–3]. The production of ROS originates from various sources, with the majority of ROS (approximately 90%) being generated by the mitochondrial respiratory chain [3, 4]. The mitochondrial electron transport chain leads to the reduction of molecular oxygen through untimely electron leakage, thereby forming superoxide and hydrogen peroxide (H_2O_2) [3, 5]. ROS, such as superoxide and H_2O_2, can activate other enzymatic systems that further stimulate ROS production and induce mitochondrial dysfunction. This leads to a vicious cycle of persistent oxidative stress and tissue damage [4, 6]. Both H_2O_2 and oxLDL have been extensively documented as inducers of oxidative damage [7–9], with in vitro experiments confirming that

they increase ROS levels and promote endothelial cell senescence [7, 10].

Telomerase reverse transcriptase (TERT), a critical component of telomerase, is known for its role in elongating telomeres and preventing replicative senescence. Beyond its classic function, TERT also reduces cellular ROS levels by binding to mitochondrial DNA (mtDNA) at the mitochondrially encoded NADH:ubiquinone oxidoreductase core subunit 1 (mt-ND1) and mitochondrially encoded NADH:ubiquinone oxidoreductase core subunit 2 (mt-ND2) coding regions, thereby enhancing respiratory chain activity. This activity is crucial for resisting oxidative damage and delaying cardiovascular aging [11–15]. Rodent studies have demonstrated TERT's protective role against oxidative damage in the cardiovascular system [13, 14, 16, 17]. The cardiovascular protective effects of TERT in humans necessitate further rigorous exploration.

Endothelial progenitor cells (EPCs), with their self-renewal capacity and ability to differentiate into mature

Zhao *et al. Journal of Translational Medicine*   (2024) 22:1080

Page 3 of 18

endothelial cells, are crucial for neovascularization and maintaining endothelial integrity and vascular homeostasis [18, 19]. Dysfunctional EPCs are linked to endothelial dysfunction and various CVD [20, 21]. Recently, Wimmer et al. developed a system using human induced pluripotent stem cells (hiPSCs) to create vascular organoids (VOs), with EPCs representing an intermediate developmental stage [22, 23]. These organoids, which feature endothelial tubes forming central cavities and interacting closely with pericytes, are enveloped by a continuous basement membrane [22]. Organoids are ideal tools for in vitro development and disease modeling due to their ability to closely replicate the cellular, spatial, and molecular architecture of human organs [24]. VOs are particularly valuable for studying vascular diseases such as diabetes and hold promise for investigating viral infections [23, 25]. Their ability to simulate the complexity of vascular tissues makes them indispensable for research into both biology and disease mechanisms.

In this study, we focus on EPCs and utilize VOs as a model to investigate the effects of oxidative stress on vascular formation. We aim to elucidate the protective role of TERT against ROS-induced oxidative damage in VOs. Additionally, we explore the interaction between TERT and UBR5, a ubiquitin protein ligase that facilitates TERT degradation through ubiquitination. We demonstrate that UBR5 knockdown leads to increased TERT levels and offers protection against oxidative damage during vascular development.

Methods

Cell culture and reagents
One line of hiPSCs was obtained from Nuwacell (RC01001-B) and cultured in complete TeSR™-E8™ medium (Stemcell, 05990). HUVECs (Sciencell, 8000) were cultured in endothelial cell medium (Sciencell, 1001). HEK293T cells were acquired from the American Type Culture Collection (Maryland, USA) and grown in Dulbecco's modified Eagle medium (Macgene, CM10013) supplemented with 10% fetal bovine serum (Excell Bio, FND500). All cells were incubated at 37 °C in a humidified atmosphere with 5% CO_2.

Treatments and stimuli
In H_2O_2 model, HUVECs were treated with 100 µM H_2O_2 or an equivalent volume of PBS for 6 h. In oxidized low-density lipoprotein (ox-LDL) model, cells were exposed to 50 µg/mL oxLDL (Yiyuan, YB-002) or 50 µg/mL native low-density lipoprotein (nLDL, Yiyuan, YB-001) for 48 h.

Plasmid construction and lentiviral production
Lentiviral vectors were constructed and packaged following established protocols [26]. PCR amplification of gene fragments was performed using the following primers: TERT forward, 5′-GCTCTAGAACCATGGCAGAGG ACTACAAGGACGACGATGACAAGTTGATGCCGC GCGCTCCCCG-3′; TERT reverse, 5′-CGGAATTCG TCCAGGATGGTCTTGAAGT-3′. Gene overexpression lentiviral vectors were created by inserting PCR-amplified fragments into pCDH-EF1-MCS-T2A-Puro (System Biosciences). Lentiviral shRNA vectors were constructed by cloning shRNA sequences into pSIH-H1-Puro (System Biosciences).

Lentiviruses were produced by cotransfecting HEK293T cells with the recombinant vectors and packaging plasmids PLP1, PLP2, or VSV-G using polyethyleneimine (PEI) transfection reagent (Selleck, E4019). The supernatant containing lentiviruses was harvested and used to infect target cells as per the manufacturer's instructions.

siRNA transfection
For siRNA transfections, Lipofectamine RNAiMAX (Thermo, 13778150) was used according to the manufacturer's protocol [27].

MitoTEMPO treatment
HUVECs were treated with 50 µM mitoTEMPO (MCE, HY-112879) dissolved in endothelial cell medium for 48 h.

VOs and treatment
VOs were generated following the method described by Dr. Wimmer et al. [22]. The hiPSCs were first washed with DPBS and then digested with Accutase Cell Dissociation Reagent (Thermo, A1110501) at 37 °C for 3 min. Cells were collected by centrifugation ($200 \times g$ for 5 min), seeded into 6-well ultralow attachment plates (5×10^5–1×10^6 cells per well), and cultured in aggregation medium (day-1). This medium comprised KnockOut DMEM/F12 (Gibco, 12660012), 20% v/v KnockOut SR-Multi-Species Serum Replacement (Gibco, 2211510), 1% v/v GlutaMAX (Gibco, 35050061), 1% v/v NEAA (Gibco, 11140035), 55 µM 2-mercaptoethanol (Gibco, 21985023), 100 U/mL penicillin–streptomycin (EallBio, 03.12001A), and 50 µM Y-27632 (Topscience, T1870).

After 24 h in aggregation medium, the cells were transitioned to N2B27 medium (day 0) consisting of neurobasal medium (Gibco, 21103049), DMEM/F12 (Gibco, 11330031) in a 1:1 ratio, 1% v/v B27 supplement (Gibco, 12587010), 0.5% v/v N2 supplement (Gibco, 17502048), 0.5% v/v GlutaMAX (Gibco, 135050061), 55 µM 2-mercaptoethanol (Gibco, 21985023), 100 U/mL penicillin–streptomycin (EallBio, 03.12001A), 12 µM CHIR99021 (Tocris Bioscience, 4423), and 30 ng/mL BMP4 (PeproTech, 120–05).

Zhao *et al. Journal of Translational Medicine*   (2024) 22:1080

Page 4 of 18

Three days later (day 3), the medium was changed to N2B27 media containing 2 μM forskolin (Sigma Aldrich, F3917) and 100 ng/mL VEGF-A (PeproTech, 10020). The aggregates were then exposed to the following treatments: 50 μM H_2O_2 or an equivalent volume of PBS for 9 h; 50 μg/mL oxLDL or 50 μg/mL nLDL for 48 h. Two days post-treatment (day 5), aggregates were embedded in Collagen I: Matrigel (1:1) gels and cultured in Stem-Pro-34 complete SFM supplemented with 15% FBS (Excell Bio, FND500), 100 ng/mL VEGF-A (PeproTech, 10020), and 100 ng/mL FGF-2 (Novoprotein, C779). Medium was replaced every 2 to 3 days. After approximately 5 days (day 10), single vascular networks were isolated using sterile syringe needles and transferred to 96-well ultralow attachment plates for additional culture for about 5 days (day 15) to complete VOs formation. Neovascular sprouting was quantified using ImageJ.

Telomeric repeated amplification protocol (TRAP) assay

Telomerase activity in VOs was assessed using the TRAPeze Telomerase Detection Kit (EMD Millipore Corp., S7700FR) according to the manufacturer's instructions. The TRAP assay, despite its limitations, is a widely recognized method for quantitative measurement of telomerase activity [28–30]. Therefore, this study also used the TRAP for quantitative analysis of telomerase activity. Briefly, VOs at different differentiation stages or cells were collected in 1.5 mL centrifuge tubes and lysed with $1 \times CHAPS$ lysis buffer (1 M Tris–HCl, 0.1 M $MgCl_2$, 1 M EGTA) on ice for 30 min. Cell lysates were then collected, and protein concentrations were determined using the BCA Protein Quantitation Assay Kit (Thermo, 23,228). For the TRAP assay, 50 ng of VOs or cell lysates were used, and the reaction products were separated on a 10% polyacrylamide gel.

Real-time quantitative polymerase chain reaction (RT-qPCR)

Total cellular RNA was extracted using TsingZol Total RNA Extraction Reagent (Tsingke, TSP401). First-strand cDNA was synthesized using HiScript III All-in-one RT SuperMix for qPCR (Vazyme, R333-01). PCR amplification of cDNA was performed with primers listed in Table S1, and β-Actin served as an internal control. Relative mRNA expression levels were determined using the comparative Ct method.

Relative mitochondrial DNA (mtDNA) content

DNA was extracted from HUVECs or VOs using an automated nucleic acid extractor (NanoMagBio, NMR0211-20) according to the manufacturer's protocol. The relative mtDNA content was detected by RT-qPCR with modifications based on previous methods [31, 32]. The routine amplification of a segment mitochondrial genomic region is conducted as a measure of mtDNA copy number (mtDNA content) [33]. The assay is based on the principle that induced DNA damage hinders the progression of DNA polymerase, leading to a decrease in the amount of PCR product [33, 34]. The mt-ND1 gene, located in the mtDNA, and the nuclear gene HGB were amplified separately. The relative mtDNA content was calculated as the ratio of mt-ND1 to HGB. Primer sequences for mt-ND1 and HGB are listed in Table S1.

RT-qPCR conditions for mt-ND1 were as follows: initial denaturation at 95 °C for 30 s, followed by 35 cycles of 94 °C for 30 s, 58 °C for 30 s, and 72 °C for 50 s; 58 °C for 5 min; 55 °C for 30 s, and 95 °C for 30 s. For HGB, the conditions were: initial denaturation at 95 °C for 30 s, followed by 35 cycles of 94 °C for 30 s, 58 °C for 30 s, 72 °C for 50 s, 58 °C for 5 min, 95 °C for 15 s, and 95 °C for 30 s.

Senescence-associated β-galactosidase (SA-β-Gal) staining

SA-β-Gal staining was conducted following the manufacturer's protocol (Cell Signaling Technology, C0602). Adherent cells or VOs slides were first fixed with 4% formaldehyde solution. The staining working solution was then applied to fully cover the tissue samples.

For adherent cells, the staining was performed at 37°C without CO_2. After staining, cells were washed with PBS and examined under a microscope. For VOs, after the initial staining, the sections were frozen. The frozen slices were subsequently stained with eosin (ZSGB-BIO, ZLI-9613) for 1–5 min, followed by dehydration through a series of ethanol concentrations (90%, 95%, and absolute ethanol) and xylene. Finally, the sections were observed under a microscope.

Co-immunoprecipitation

Cells were lysed with immunoprecipitation (IP) buffer (50 mM Tris–HCl, pH 7.4; 1% Triton X-100; 0.5 mM EDTA; 150 mM NaCl; 10% glycerol; 40 mM 2-mercaptoethanol) on ice for 30 min to obtain whole-cell lysates. Anti-Myc Affinity Gel (Beyotime, P2285) or FLAG M2 monoclonal antibody affinity gel (Sigma Aldrich, A2220) was then added to the lysates and incubated overnight at 4 °C. The beads were washed 3 times with IP buffer and then resuspended in $2 \times SDS$ sample buffer. The samples were analyzed by Western blotting.

Western blot

Cells were collected in 1.5 mL centrifuge tubes and lysed on ice for 30 min using RIPA lysis buffer (150 mM NaCl, 1.0% NP-40, 0.5% sodium deoxycholate, 0.1% SDS, 50 mM Tris, pH 8.0). Protein concentrations in the whole-cell lysates were quantified using the BCA Protein Quantification Assay Kit (Thermo, 23228). Equal

Zhao *et al. Journal of Translational Medicine*   (2024) 22:1080

Page 5 of 18

amounts of protein were separated by 8% or 12% SDS-PAGE and transferred to nitrocellulose membranes.

The membranes were blocked with TBST (containing 5% skim milk) for 1 h at room temperature and then incubated overnight at 4 °C with the following primary antibodies: anti-Cyclin D1 (ProteinTech, 60186-1-Ig, 1:1000), anti-Cyclin B (Santa Cruz, SC166210, 1:200), anti-p53 (Millipore, 05-224, 1:5000), anti-β-Actin (ProteinTech, HRP-60008, 1:10,000), anti-Flag-tag (Sigma Aldrich, A8592, 1:5000), anti-Myc-tag (MBL, M047-7, 1:3000), anti-p21 (ProteinTech, 10355-1-AP, 1:1000), and anti-Ub (MBL, D071-3, 1:500).

After incubation with primary antibodies, the membranes were washed with TBST and then incubated with appropriate secondary antibodies before detection.

Ubiquitination assay

HUVECs stably expressing Flag-tagged TERT (HUVEC-Flag-TERT) were transfected with either Myc-UBR5 or Myc-tag control using PEI. The cells were then treated with 10 μM MG132 (Apexbio, A2585) for 36 h prior to harvesting. In separate experiments, HUVEC-Flag-TERT cells were transfected with either siUBR5 or a non-targeting control (siNC) using RNAiMAX, followed by transfection with Myc-UBR5 or Myc-tag using PEI according to the manufacturer's protocol. After 2 days, these cells were further transfected with HA-Ubiquitin and treated with 10 μM MG132 (Apexbio, A2585) for 6 h before harvesting. Cell lysates were immunoprecipitated with anti-Flag beads and analyzed by Western blotting using anti-Ub antibody (MBL, D071-3, 1:500) and anti-Flag-tag antibody (Sigma Aldrich, A8592, 1:5000).

Immunofluorescence (IF)

For VOs, whole-mount or 10 μm slices were fixed with 4% paraformaldehyde and incubated in blocking buffer (3% FBS, 1% BSA, 0.5% Triton X-100, 0.5% Tween 20, 0.01% sodium deoxycholate) for 2 h at room temperature. Subsequently, the samples were incubated overnight at 4 °C with primary antibodies.

The following primary antibodies were used: anti-platelet endothelial cell adhesion molecule-1 (CD31) (Cell Signaling Technology, 3528S, 1:100), anti-platelet-derived growth factor receptor beta (PDGFR-β) (Cell Signaling Technology, 3169S, 1:100), anti-collagen IV (Col IV) (R&D, ab19808, 1:100), anti-alpha smooth muscle actin (α-SMA) (Cell Signaling Technology, 19245S, 1:200), Alexa Fluor® 488 anti-α-SMA (Abcam, ab184675, 1:200), anti-p16^{Ink4a} (ProteinTech, 10883-1-AP, 1:100), anti-UBR5 (ProteinTech, 22782-1-AP, 1:100), and anti-Flag-tag (Sigma Aldrich, F1804, 1:100).

After primary antibody incubation, samples were treated with fluorescent secondary antibodies: Alexa Fluor™ 594-conjugated anti-rabbit IgG (Invitrogen, A-11012, 1:500), Alexa Fluor™ 488-conjugated anti-rabbit IgG (Invitrogen, A-11008, 1:500), Alexa Fluor™ 594-conjugated anti-mouse IgG (Invitrogen, A-11005, 1:500), and Alexa Fluor™ 488-conjugated anti-mouse IgG (Invitrogen, A-11001, 1:500). Nuclei were stained with DAPI.

Confocal images were acquired using a Zeiss LSM880 microscope. The excitation and emission wavelengths were 590/617 nm for red fluorescence and 498/520 nm for green fluorescence.

MitoSOX mitochondrial superoxide assay

Mitochondrial superoxide levels in HUVECs were assessed using the MitoSOX™ Red Mitochondrial Superoxide Indicator (Invitrogen, M36008) following the manufacturer's instructions. Briefly, cells were incubated with 2 μM MitoSOX Red in Hank's buffer for 30 min at 37°C in a 5% CO_2 atmosphere. After incubation, superoxide fluorescence was detected using fluorescence microscopy with an excitation wavelength of 590 nm and an emission wavelength of 617 nm.

5-Ethynyl-2′-deoxyuridine (EdU) incorporation assay

Cell proliferation was measured using the BeyoClick™ EdU Cell Proliferation Kit with Alexa Fluor 488 (Beyotime, C0071S) or 594 (Beyotime, C0078S) following the manufacturer's protocol. Cells were cultured overnight, then incubated with EdU working solution (10 μM) for 8 h. After EdU labeling, the culture medium was removed and cells were fixed with 4% paraformaldehyde for 15 min at room temperature.

Following fixation, cells were treated with Click Additive Solution for 30 min in the dark at room temperature. The cells were then washed three times with PBS containing 0.3% Triton X-100 and stained with Hoechst 33342 for nuclear visualization. Fluorescence images were acquired for detection.

Statistical analysis

Sample sizes were determined based on previous trials or similar experiments to ensure sufficient statistical power. Data analysis and graphical representation were conducted using GraphPad Prism 9.5.1, IBM SPSS Statistics 26.0, and Adobe Illustrator 27.0. Data that followed a normal distribution are presented as mean ± standard deviation (SD), while data that did not follow a normal distribution are presented as median ± interquartile range (IQR).

The significance of differences between two groups with normally distributed data and equal variances was assessed using Student's t-test. For normally distributed data with unequal variances, Welch's t-test was used.

Zhao *et al. Journal of Translational Medicine*   (2024) 22:1080

Page 6 of 18

For non-normally distributed data, the Wilcoxon rank-sum test was applied. For comparisons among multiple groups, one-way ANOVA was used when data were normally distributed and variances were homogeneous, followed by Fisher's Least Significant Difference (LSD) test for post-hoc analysis. When data met the normality assumption but did not exhibit homogeneity of variances, Welch's ANOVA was employed, followed by Dunnett's T3 test for multiple comparisons. Non-normally distributed data with multiple groups were analyzed using the Kruskal–Wallis test followed by Dunn's test. A *P*-value of < 0.05 was considered statistically significant for all tests. Each experiment was repeated at least three times.

Results

ROS impairs VO development and induce cellular senescence

The development of VOs follows a series of stages: aggregate formation, mesoderm induction, vascular lineage induction, vascular network formation, and maturation into fully developed VOs (Fig. 1A). On day 3, stem cells progress to the streak/early mesoderm-like stage [35]. By day 4, the number of EPCs in VOs peaks [35]. EPCs are known to promote endothelial cell (EC) differentiation and vascular network formation both in vitro and in vivo [36]. By day 10, highly migratory ECs, termed tip cells, guide the proliferation of stalk cells, facilitating the formation of new radial vessels. By day 15, these radial vessels merge to establish a closed vascular network. The ECs, identified by CD31, organize into dense vascular networks. This network comprises pericytes, marked by PDGFR-β, smooth muscle cells, identified by α-SMA, and a basement membrane, indicated by Col IV (Fig. 1B; Fig. S1).

 ROS are highly reactive molecules that can modulate various cellular functions; but excessive ROS can cause vascular damage [37]. To evaluate ROS-induced damage in VOs, we exposed them to H_2O_2 and oxLDL at the EPC stage and analyzed the organoids at subsequent intervals (Fig. 1C and Fig. S2). Neovascular sprouting

in VOs, characterized by radial outgrowths of blood vessels driven by tip cells, was significantly reduced in the H_2O_2-treated and oxLDL-treated group, indicating impaired angiogenic potential (Fig. 1D, Fig. S2A). Additionally, exposure to H_2O_2 or oxLDL resulted in an increased the proportion of senescent cells compared to the PBS-treated group (Fig. 1E, Fig. S2B). H_2O_2 treatment also elevated levels of p16^{INK4a}, a marker of cellular senescence (Fig. 1F) [38]. Furthermore, VOs treated with H_2O_2 exhibited higher secretion of senescence-associated secretory phenotype proteins (SASPs), such as C-X-C motif chemokine ligand 1 (CXCL1) and matrix metalloproteinase 1 (MMP1)(Fig. 1G). The damage of mtDNA is caused by the lack of protective histones in its structure and the absence of effective repair mechanisms. Mitochondrial DNA is susceptible to oxidative damage by ROS, leading to the formation of deoxyribose rings, apurinic/apyrimidinic sites, strand breaks, and other types of damage [33, 39]. To investigate mtDNA damage, we used qRT-PCR to determine the mtDNA content. The VOs treated with H_2O_2 have a lower mtDNA content compared to those treated with PBS (Fig. 1H). These findings collectively demonstrate that ROS exposure impairs VO angiogenic potential, disrupts development, and accelerates cellular senescence.

TERT alleviates oxidative stress-induced senescence in HUVECs

H_2O_2 or oxLDL treatment induces increased senescence in ECs [10, 40], evidenced by reduced cell growth, proliferation, angiogenesis, and increased SA-β-Gal activity [41]. H_2O_2 increased ROS levels and exacerbated HUVEC senescence (Fig. 2). Treatment with 50 μg/mL of nLDL did not induce significant senescence, whereas the same concentration of oxLDL increased SA-β-Gal activity and senescence-related proteins such as p21, reflecting augmented ROS production (Fig. S3). H_2O_2 or oxLDL (with nLDL as a control) were therefore employed to enhance oxidative stress levels. To assess the protective role of TERT, a stable HUVEC line expressing

(See figure on next page.)

Fig. 1 ROS impairs VO development and induces cell senescence. **A** Schematic timeline and landmark stages of VO development from hiPSCs: aggregates (day 0), mesoderm (day 3), vascular lineage (day 5), vascular networks (day 10), and VOs (day 15). Scale bar, 450 μm. **B** IF of VOs. CD31 (red) labels endothelial cells, PDGFR-β (green) labels mural cells, Col IV (red) labels the basement membrane, α-SMA (green) labels vascular smooth muscle cells, and DAPI (blue) stains nuclei. Scale bar, 250 μm (day 15). **C** Schematic timeline for H_2O_2 treatment of VOs: 50 μM H_2O_2 was applied for 9 h at the vascular lineage stage (day 4). **D** Microscopic images of VOs (day 10) after treatment with 50 μM H_2O_2 or PBS for 9 h at the vascular lineage stage. Arrows indicate neovascular sprouting. Relative sprouting counts were analyzed using ImageJ. Scale bar, 250 μm. **E** SA-β-Gal staining of VOs (day 15). The percentage of SA-β-Gal-positive cells was calculated as the area of SA-β-Gal staining (blue) relative to eosin-stained area (red). The values were obtained from five randomly selected fields. Scale bar, 50 μm. **F** IF of VOs showing p16^{INK4a} (green) as a marker of senescent cells, with DAPI (blue) staining nuclei. Scale bar, 60 μm. Relative p16^{INK4a} fluorescence intensity was quantified from five randomly selected fields. **G** Relative SASP (CXCL1, MMP1) levels in VOs assessed by RT-qPCR. **H** Relative mtDNA content in VOs measured by RT-qPCR. (ns, not significant; **$P < 0.01$; ***$P < 0.001$)

Zhao et al. Journal of Translational Medicine   (2024) 22:1080

Page 7 of 18
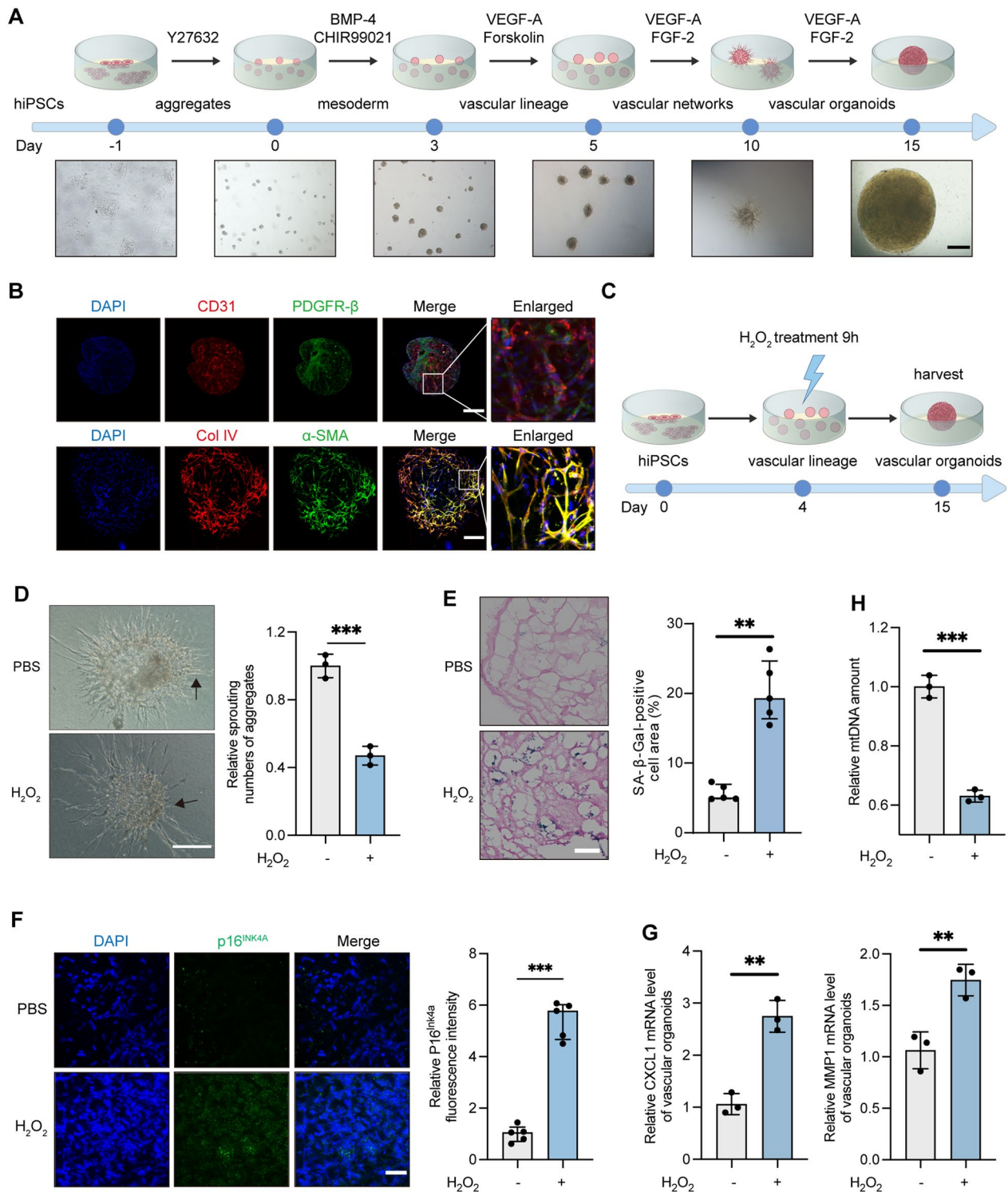
Fig. 1 (See legend on previous page.)

Flag-tagged TERT (HUVEC-Flag-TERT) was constructed (Fig. 2A). TERT overexpression markedly alleviated senescence induced by H_2O_2 or oxLDL, as indicated by reduced SA-β-Gal activity (Fig. 2B, Fig. S4A). This was supported by the 5-ethynyl-2'-deoxyuridine (EdU) incorporation assay, showing preserved proliferation in

Zhao *et al. Journal of Translational Medicine*   (2024) 22:1080

Page 8 of 18
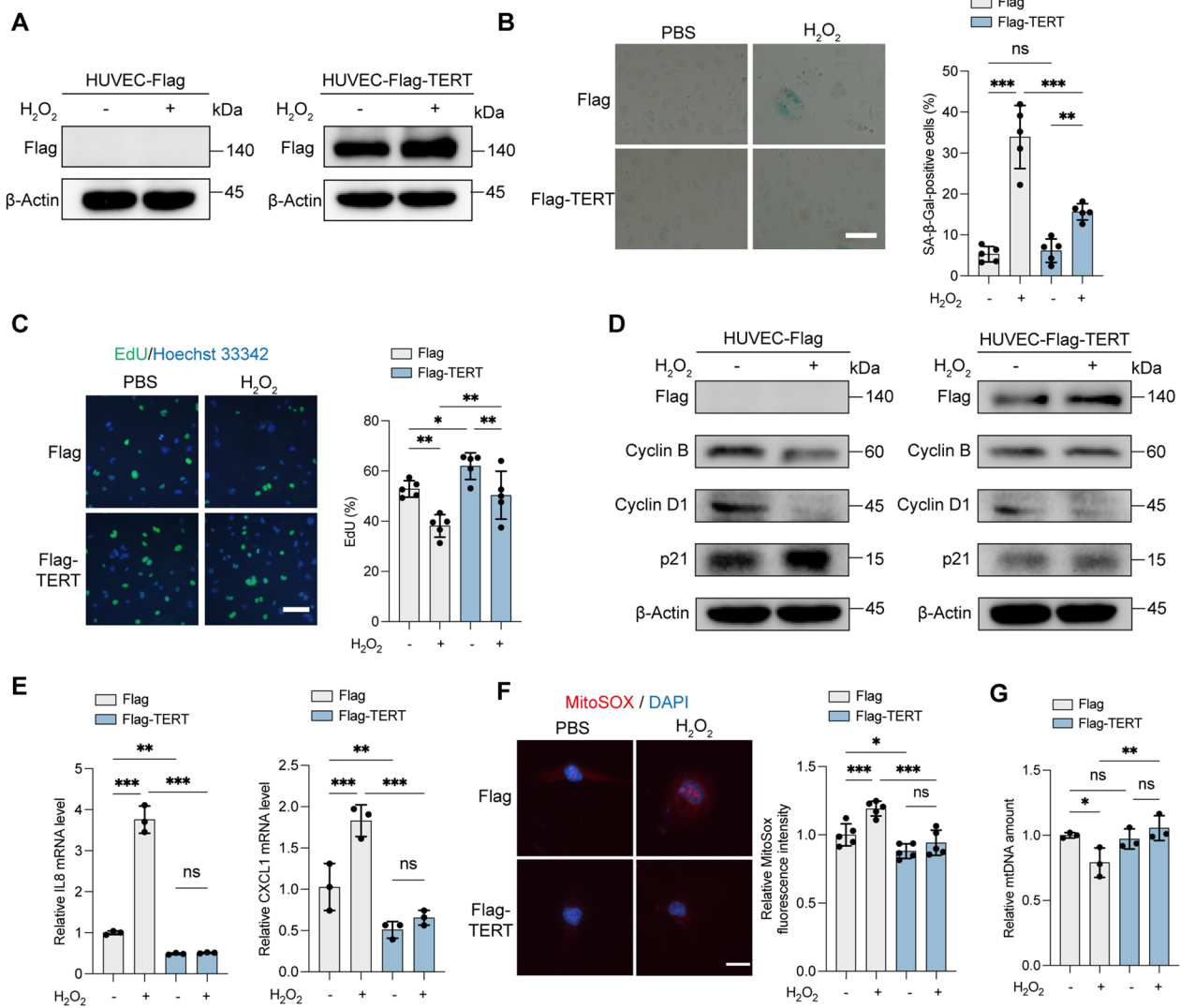
Fig. 2 TERT alleviates ROS-induced senescence and ROS production in HUVECs. **A–G** HUVEC-Flag and HUVEC-Flag-TERT cells were treated with 100 μM H_2O_2 or PBS for 6 h. **A** Western blot analysis showing Flag levels in cell lysates from HUVEC-Flag and HUVEC-Flag-TERT cells. **B** Representative images of SA-β-Gal staining. The percentage of SA-β-Gal-positive cells was quantified from five random fields. Scale bars, 150 μm. **C** EdU incorporation assay. Cells were labeled with EdU (green) and stained with Hoechst 33342 (blue) for nuclei. The percentage of EdU-positive cells was quantified from five random fields. Scale bars, 75 μm. **D** Western blot analysis of Flag, Cyclin B, Cyclin D1, and p21 in cell lysates from HUVEC-Flag and HUVEC-Flag-TERT cells. β-Actin was used as an internal control protein. **E** Relative SASP (IL8, CXCL1) levels measured by RT-qPCR in HUVEC-Flag and HUVEC-Flag-TERT cells. **F** MitoSOX Red staining to assess mitochondrial superoxide levels. Nuclei were labeled with DAPI (blue). Scale bars, 20 μm. The relative MitoSOX fluorescence intensity was quantified from five random fields. **G** Relative mtDNA content of HUVEC-Flag or HUVEC-Flag-TERT cells determined by RT-qPCR. (ns, not significant; *$P < 0.05$; **$P < 0.01$; ***$P < 0.001$)

HUVEC-Flag-TERT cells post-treatment (Fig. 2C, Fig. S4B). Additionally, Cyclin B, Cyclin D1, and p21 levels were less affected by H_2O_2 in HUVEC-Flag-TERT compared to HUVEC-Flag cells (Fig. 2D). The oxLDL treatment did not significantly increase p21 and p53 levels in Flag-TERT-expressing HUVECs (Fig. S4C). Oxidative stress led to elevated SASP factors, including interleukin-8 (IL8) and CXCL1, in HUVEC-Flag cells; however, SASP levels in HUVEC-Flag-TERT cells were lower,

with minimal accumulation of IL8 and CXCL1 following H_2O_2 treatment (Fig. 2E). MitoSOX staining revealed reduced mitochondrial ROS generation in HUVEC-Flag-TERT compared to HUVEC-Flag cells post-H_2O_2 treatment (Fig. 2F). Moreover, mtDNA content decreased in HUVEC-Flag cells after H_2O_2 exposure, whereas HUVEC-Flag-TERT cells showed no significant change (Fig. 2G). Administration of mitoTEMPO, a mitochondrial ROS scavenger, negated the effects of H_2O_2 on

SA-β-Gal activity (Fig. S5). Collectively, these results suggest that TERT protects against mitochondrial oxidative stress, stabilizes mtDNA, and mitigates oxidative stress-induced cellular senescence.

TERT alleviates ROS-induced VO impairment and cellular senescence

During mammalian development, TERT expression decreases with cell differentiation and maturation. TERT mRNA and telomerase activity were present prior to vascular lineage induction but declined as aggregates formed and developed. By the vascular network and VO stages, these levels were undetectable (Fig. 3A, B).

To explore TERT's antioxidant and anti-senescence effects, we generated VOs from hiPSCs stably expressing Flag-TERT or Flag and subjected them to oxidative stress induced by H_2O_2 during the EPC stage (Fig. 3C, D). Flag-TERT expression preserved the vascular sprouting ability of VOs under H_2O_2 exposure (Fig. 3E). H_2O_2 treatment increased SA-β-Gal activity in VOs from hiPSC-Flag cells; however, VOs expressing Flag-TERT showed significantly reduced SA-β-Gal activity, despite increase in ROS (Fig. 3F). Additionally, Flag-TERT counteracted the ROS-induced upregulation of p16INK4A (Fig. 3G). These results indicate that Flag-TERT overexpression alleviates ROS-induced VO impairment and cellular senescence.

UBR5 interacts with TERT and participates its ubiquitin-mediated degradation

To further explore factors influencing TERT level and function, we employed co-immunoprecipitation (Co-IP) combined with mass spectrometry (MS) to identify proteins interacting with Flag-tagged TERT (Flag-TERT) in HUVECs. MS analysis revealed several interacting proteins, including heat shock protein 70 (HSP70), UBR5, heterogeneous nuclear ribonucleoprotein R (HNRNPR), and melanoma-associated antigen D2 (MAGED2) (Fig. 4A, B). Notably, UBR5 stood out as it is part of the E3 ligase complex (UBR5, DDB1, and VprBP, collectively known as EDVP) previously reported to interact with TERT and facilitate its ubiquitin-mediated degradation [42]. We confirmed the interaction of UBR5 and TERT (Fig. 4C, D). Pescadillo ribosomal biogenesis factor 1 (PES1), a known telomerase assembly factor that interacts with TERT [27], was used as a positive control (Fig. 4C).

We then investigated whether UBR5 regulates TERT levels by knocking down UBR5 in Flag-TERT overexpressing HUVECs, as endogenous TERT is typically present in very low amounts (∼500 molecules per cell, even in cancer cells) and antibodies for its detection are limited [43]. We observed an increase in Flag-TERT levels in UBR5-knockdown cells (Fig. 4E, F). To determine if UBR5 mediates TERT degradation via the ubiquitin–proteasome pathway, we treated cells with the proteasome inhibitor MG132, which blocked UBR5-induced Flag-TERT degradation (Fig. 4G, H). Additionally, in HUVECs stably expressing Flag-TERT, transient transfection with HA-Ub followed by MG132 treatment showed increased Ub-tagged Flag-TERT levels after Myc-UBR5 transfection. Conversely, UBR5 siRNA transfection led to a decrease in Ub-tagged Flag-TERT levels (Fig. 4I, J). In summary, UBR5 mediates TERT degradation via the ubiquitin–proteasome pathway.

Inhibition of UBR5 protects VOs from oxidative stress-induced senescence or damage

We next explored whether modulating UBR5 levels in EPCs could prevent oxidative stress, delay cellular senescence, and mitigate ROS-induced damage in VOs. To achieve this, we constructed hiPSCs stably expressing UBR5 shRNA (hiPSC-shUBR5) to inhibit UBR5 expression and then differentiated these cells into VOs (Fig. 5A, B, Fig. S6). During vascular lineage induction, we exposed the EPCs to H_2O_2 to induce oxidative stress in the VOs (Fig. 5A, B). UBR5 knockdown preserved the angiogenic sprouting capacity of VOs under H_2O_2 treatment (Fig. 5C). Inhibition of UBR5 also reversed the increase in SA-β-Gal activity and mitigated the progression of senescence in VOs exposed to H_2O_2 (Fig. 5D). Additionally, UBR5 knockdown reduced the upregulation of p16INK4a and SASP factors (IL8 and CXCL1), and alleviated the reduction of mtDNA content caused by H_2O_2 in VOs (Fig. 5E–G). UBR5 siRNA transfection consistently increased the Flag-TERT levels in hiPSCs and vascular lineages, with or without exposure to H_2O_2 (Fig. 5H, I). These results suggest that inhibiting UBR5 alleviates oxidative stress-induced impairment in VOs.

To further investigate whether the protective effects of UBR5 inhibition are mediated through TERT, we analyzed the impact of UBR5 knockdown in HUVECs transfected with an empty vector or Flag-TERT (Fig. 6A, Fig. S7A). Telomerase activity is a hallmark of undifferentiated iPSCs, thus, without it they are no functional iPSCs. Given that TERT is essential for the long-term culture and pluripotency of hiPSCs [44, 45], culturing VOs from hiPSCs lacking TERT was not feasible (data not shown). In our model system, we have not detected the presence of TERT expression or telomerase activity in endothelial cells. As anticipated, UBR5 knockdown did not rescue ROS-induced senescence in HUVECs transfected with the empty vector but significantly alleviated senescence in HUVECs expressing Flag-TERT (Fig. 6B, Fig. S7B). Additionally, UBR5 knockdown alleviated the reduction of ROS-induced EdU incorporation (Fig. 6C, Fig. S7C),
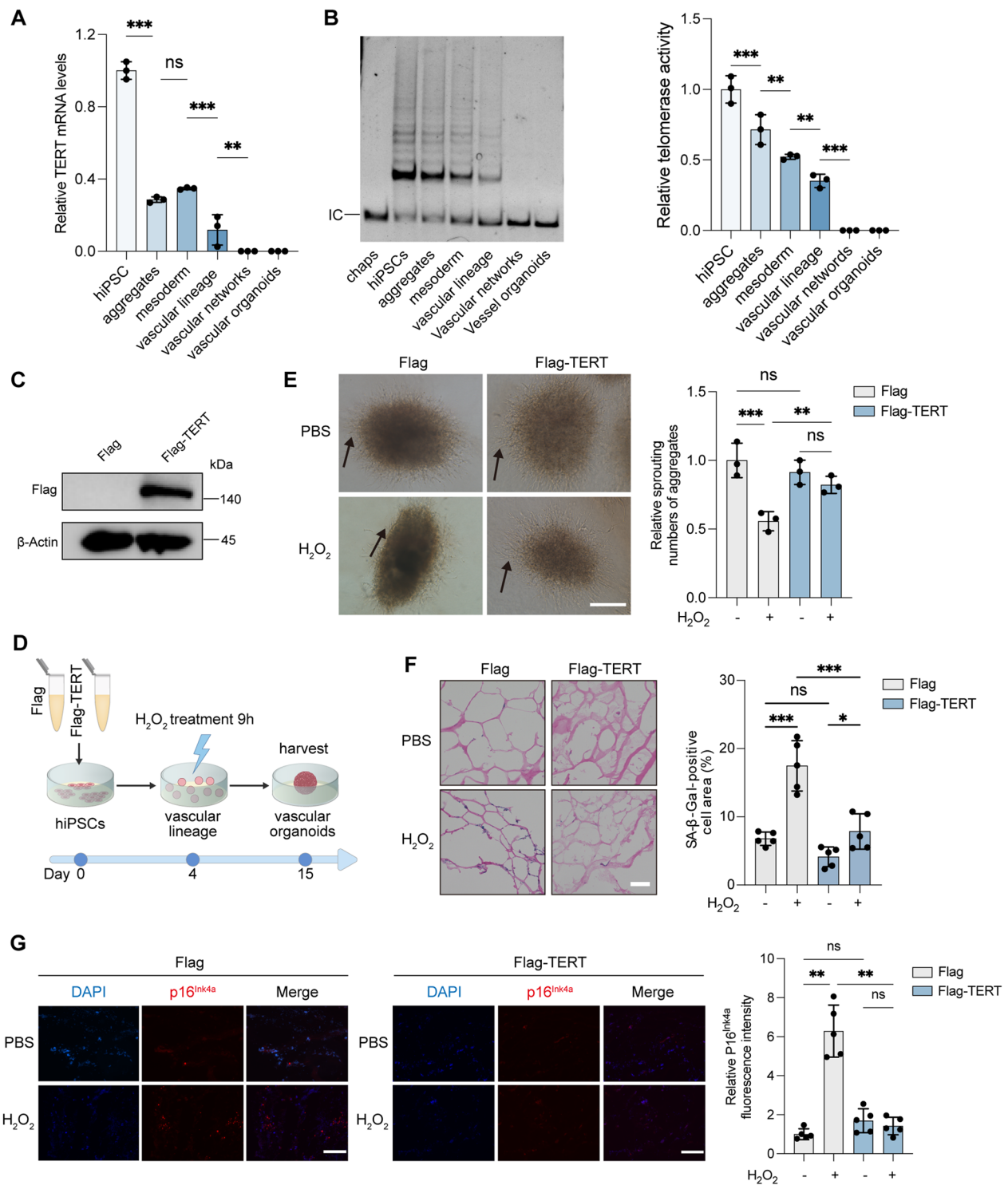
Fig. 3 TERT alleviates ROS-induced impairment and senescence in VOs. **A** Relative TERT mRNA levels in VOs during development, measured by RT-qPCR. **B** Telomerase activity assessed by the telomerase repeat amplification protocol (TRAP). CHAPS lysate served as a negative control. **C** Western blot analysis of Flag levels in hiPSCs. **D** Schematic timeline of H_2O_2 treatment in VOs. **E** Microscopic images of VOs (day 10) following 50 μM H_2O_2 or PBS treatment. Arrows indicate neovascular sprouting. Scale bars, 250 μm. **F** SA-β-Gal staining of VOs (day 15). Scale bars, 50 μm. The percentage of SA-β-Gal-positive cell area (blue) relative to eosin-stained area (red) was calculated from five random fields. **G** IF of VOs for p16^{INK4a} (red) and DAPI (blue) staining. Scale bars, 50 μm. Relative p16^{INK4a} fluorescence intensity was calculated from five random fields. (ns, not significant; $*P < 0.05$; $**P < 0.01$; $***P < 0.001$)
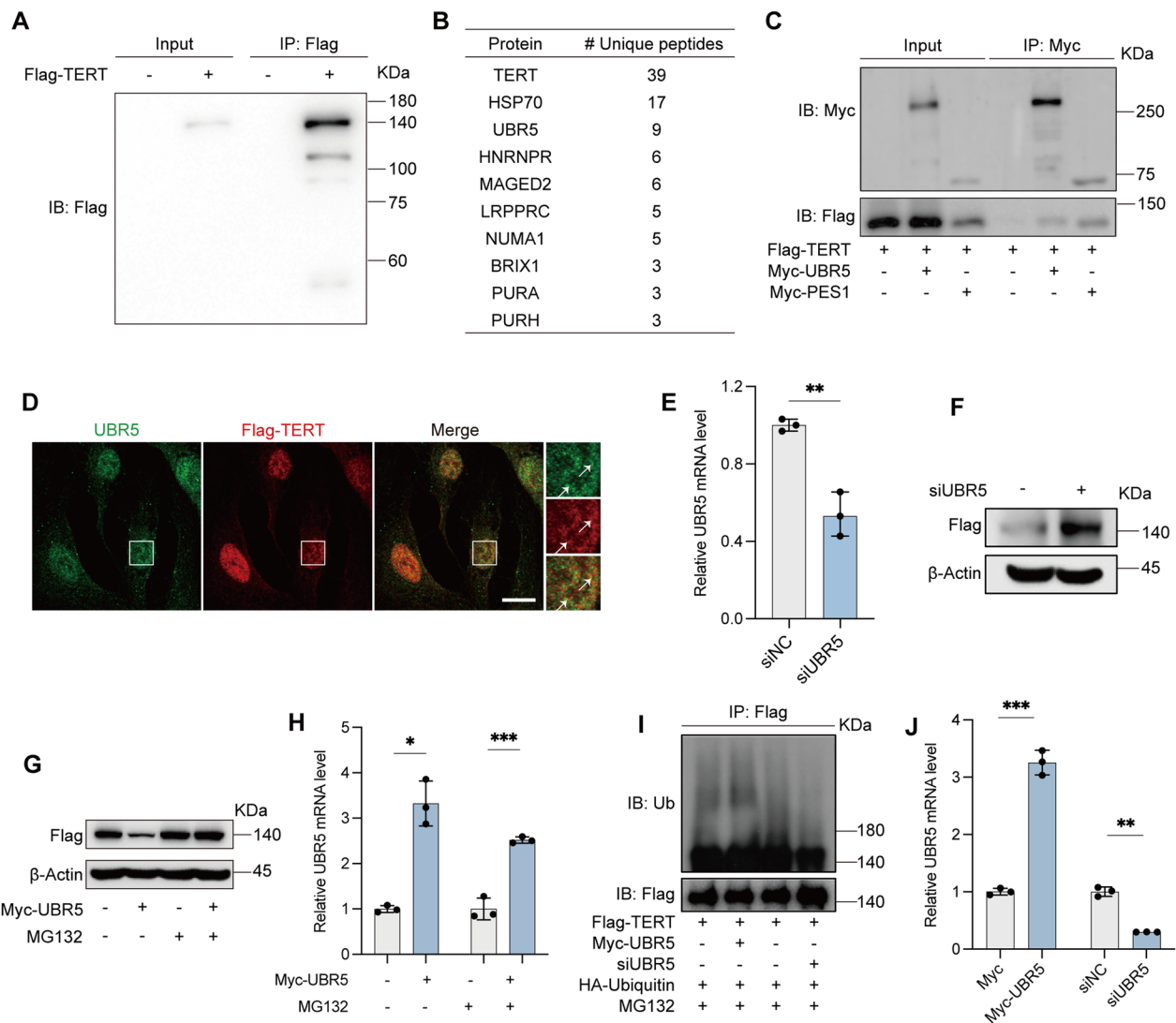
Fig. 4 UBR5 interacts with TERT, and its knockdown stabilizes TERT. **A** Whole-cell lysates from HUVEC-Flag and HUVEC-Flag-TERT cells were subjected to immunoprecipitation (IP) with an anti-Flag antibody, followed by immunoblotting (IB) with an anti-Flag antibody. **B** Cell extracts from HUVECs stably expressing Flag or Flag-tagged TERT (Flag-TERT) were immunopurified with an anti-Flag affinity gel, and the purified complexes were analyzed by SDS-PAGE. Differential protein bands were retrieved and identified by MS. **C** Cells transiently transfected with Myc-UBR5 or Myc-PES1 were immunoprecipitated (IP) with an anti-Myc antibody, followed by IB with the indicated antibodies. Myc-PES1 served as a positive control for Co-IP. **D** IF of HUVEC-Flag-TERT for UBR5 (green) and Flag-TERT (red) staining. Arrows indicate the colocalization of UBR5 with Flag-TERT. Scale bars, 15 μm. **E**, **F** HUVEC-Flag-TERT cells were transiently transfected with siUBR5 or siNC. **E** Relative UBR5 mRNA levels were determined by RT-qPCR. **F** Representative western blot of Flag levels in cell lysates. β-Actin was used as an internal control. **G**, **H** HUVEC-Flag or HUVEC-Flag-TERT cells transiently transfected with Myc-UBR5 or Myc-tag were treated with 10 μM MG132 for 36 h prior to harvesting. **G** Representative western blot showing Flag levels in cell lysates. β-Actin served as an internal control. **H** Relative UBR5 mRNA levels were measured by RT-qPCR. **I**, **J** HUVEC-Flag-TERT cells were transiently transfected with HA-ubiquitin (HA-Ub) and Myc-UBR5 or siUBR5 were treated with 10 μM MG132 for 6 h before harvesting. **I** Whole-cell lysates were subjected to IP with an anti-Flag antibody, followed by IB with the indicated antibodies. **J** Relative UBR5 mRNA levels were assessed by RT-qPCR. (ns, not significant; *$P < 0.05$; **$P < 0.01$; ***$P < 0.001$)

reduced mitochondrial superoxide level (Fig. 6D), and alleviated the reduction of mtDNA content (Fig. 6E) in Flag-TERT-expressing HUVECs. Collectively, these findings indicate that shUBR5 counteracts oxidative stress-induced senescence through TERT, with UBR5

Zhao *et al. Journal of Translational Medicine*   (2024) 22:1080

Page 12 of 18

inhibition providing protection against oxidative damage in VOs.

Discussion

In the present study, we investigated the effect of mitochondrial ROS on VO development and cellular senescence, and assessed the protective effects of the UBR5/TERT axis on these processes. We adapted the 3D VO creation technique initially developed by Wimmer and colleagues [22], successfully establishing a robust culture system. This approach builds on the 2D co-culture system established by Orlova et al. in 2014 [46], which used hiPSCs to co-culture ECs and pericytes, facilitating the formation of a primary vascular plexus. This system enabled the cells to autonomously develop an endothelial network through their interactions [47]. VOs offer a novel 3D vascular network system that closely replicates the morphology, function, and molecular characteristics of human microvessels. They effectively model the interactions between ECs and pericytes, the formation of vascular lumens, and basement membrane deposition. This innovative model holds significant promise for advancing personalized precision medicine. VOs have potential applications across various domains, including organ development research [22], studying the pathophysiology of secondary vascular diseases, modeling rare inherited vascular disorders, and drug screening [23]. Additionally, VOs could be utilized in clinical organ transplantation strategies [48]. Given that the vasculature is influenced by diverse physiological and environmental factors, VO models can serve as valuable alternatives or surrogates to in vivo experiments that may not meet ethical standards.

In our study, we utilized the VO model to explore EPC function under conditions of increased oxidative stress, induced by H_2O_2 or oxLDL. Elevated ROS levels compromised the vasculogenic capacity of EPCs and accelerated cellular senescence in VOs. Our findings are consistent with previous studies; for instance, Nikolova et al. [35] reported that perturbation of the vascular endothelial growth factor (VEGF) and Notch signaling pathways in VOs influences vascular network sprouting and proliferation. Specifically, inhibition of the Notch pathway leads to impaired endothelial cell–cell interactions and reduced vessel formation [35]. In addition, VOs were exposed to elevated glucose, tumor necrosis factor (TNF), and interleukin-6 (IL-6) levels to effectively model diabetic vasculopathy [23]. These VOs exhibited a reduction in endothelial and pericyte numbers, along with thickened and multilayered basement membranes, similar to changes observed in the vasculature of type 2 diabetes patients [23]. VO models have been instrumental in elucidating the role of glycolysis in ECs and the effects of metabolic modulation on the vasculature [49]. Inhibition of glycolysis in endothelial cells within VO models leads to vascular remodeling, characterized by reduced pericyte coverage, vessel density, and vessel length [49].

Previous study reported a notable increase in EPCs on the fourth day of VO development [35]. EPCs are critical for maintaining endothelial integrity and vascular homeostasis [20, 21, 36, 50, 51]. Dysfunctional EPCs are implicated in endothelial dysfunction and various cardiovascular conditions, including atherosclerosis, hypertension, and stroke [20, 21]. Vascular progenitor cells respond to mobilization signals by producing proangiogenic and growth factors, which stimulate the proliferation and migration of existing endothelial cells, thereby supporting vascular regeneration and tissue homeostasis. However, elevated oxidative stress not only diminishes the number of endothelial cells but also impairs EPC functionality. For instance, in a rat model of myocardial infarction, increased ROS production was associated with a reduction in EPC numbers [50]. Conversely, $Nox2^{-/-}$ mice, which exhibit reduced ROS production and lower oxidative stress levels in ischemic tissues, demonstrate enhanced EPC migration and adhesion [51].

Our study elucidates the role of TERT in maintaining vascular redox homeostasis in humans. We found that overexpression of TERT mitigated the impairment of neovascular sprouting and reduced cellular senescence in VOs exposed to increased oxidative stress. Traditionally,

(See figure on next page.)

Fig. 5 Inhibition of UBR5 alleviates ROS-induced VO impairment. **A** Schematic timeline of H_2O_2 treatment of VOs. hiPSCs expressing shNC or shUBR5 were subjected to 50 µM H_2O_2 or PBS for 9 h at the vascular lineage stage (day 4). **B** Relative UBR5 mRNA levels in hiPSCs and VOs were assessed by RT-qPCR. **C** VOs were imaged after treatment with 50 µM H_2O_2 or PBS for 9 h at the vascular lineage stage (day 10). Arrows indicate neovascular sprouting. Scale bars: 300 µm. Sprouting numbers were quantified using ImageJ. **D** SA-β-Gal staining of VOs at day 15. Scale bars: 50 µm. The percentage of SA-β-Gal-positive cell area (blue) relative to eosin-stained area (red) was quantified. The values were obtained from five randomly selected fields. **E** IF staining of VOs for p16^INK4a (green) to mark senescent cells, with DAPI (blue) for nuclei. Scale bars: 250 µm. p16^INK4a fluorescence intensity was quantified from five randomly chosen fields. **F** Relative SASP (IL8, CXCL1) levels in VOs determined by RT-qPCR. **G** Relative mtDNA levels in VOs determined by RT-qPCR. **H-I** hiPSC-Flag-TERT cells were transiently transfected with siNC or siUBR5, followed by treatment with 50 µM H_2O_2 or PBS. **H** Western blot analysis showing Flag levels in lysates from hiPSC-Flag-TERT (left). Relative UBR5 mRNA levels were assessed by RT-qPCR (right). **I** Western blot analysis showing Flag levels in lysates from vascular lineage developed from hiPSC-Flag-TERT (left). Relative UBR5 mRNA levels were assessed by RT-qPCR (right). (ns, not significant; *$P < 0.05$; **$P < 0.01$; ***$P < 0.001$)
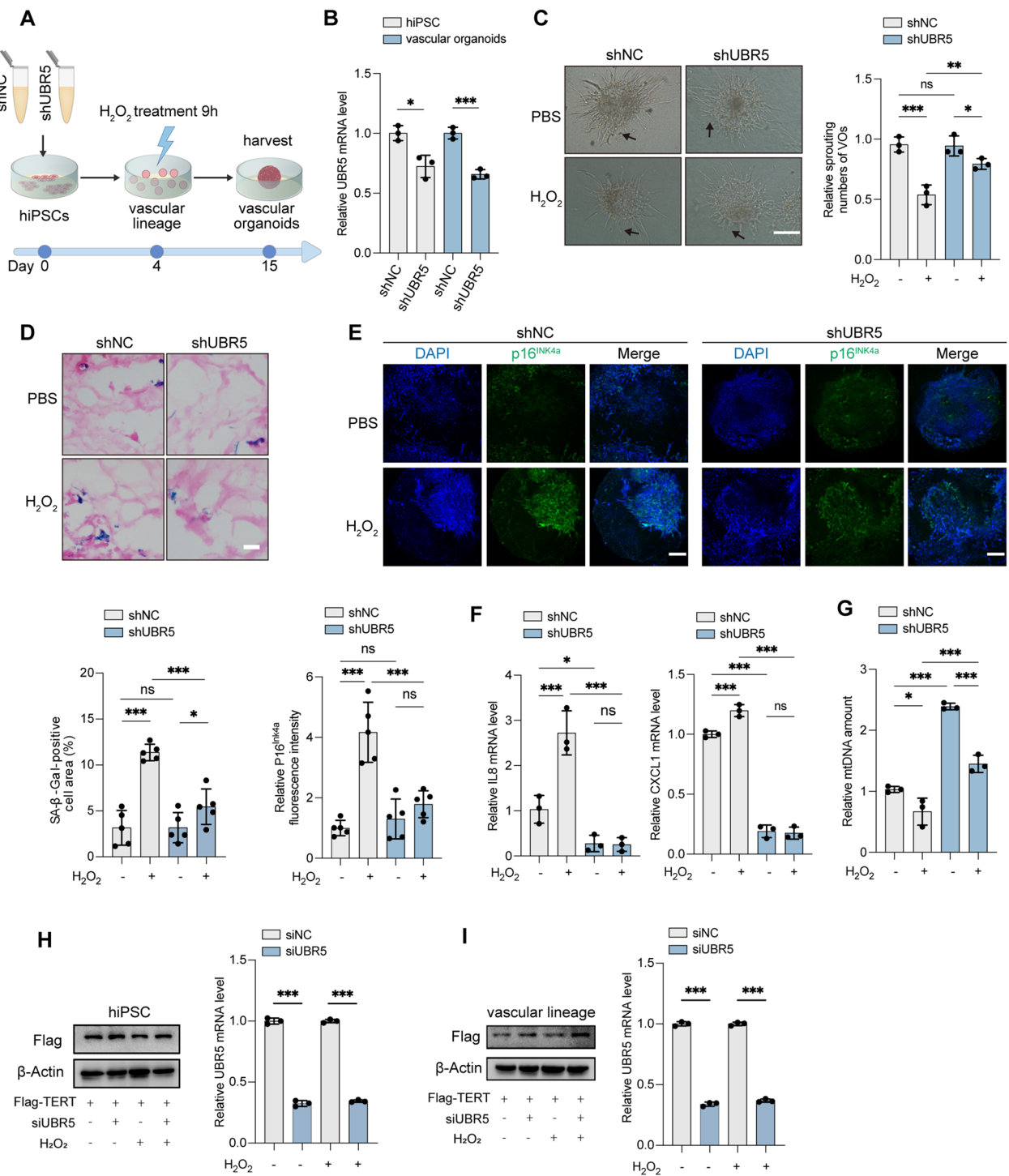
Fig. 5 (See legend on previous page.)

telomerase is recognized primarily for its role as a tel-omere ribonucleoprotein reverse transcriptase, which extends telomeres, maintains genome stability, and sup-ports unlimited cellular proliferation potential. While tel-omerase RNA (TERC), harbors the telomerase template

sequence, is ubiquitously expressed, the presence of TERT in the cardiovascular system is a matter of contro-versy. Some studies have indicated that TERT is primar-ily found in germ cells and stem cells in humans, and is generally not detected in HUVECs [52–55]. Conversely,

Zhao *et al. Journal of Translational Medicine*   (2024) 22:1080

Page 14 of 18
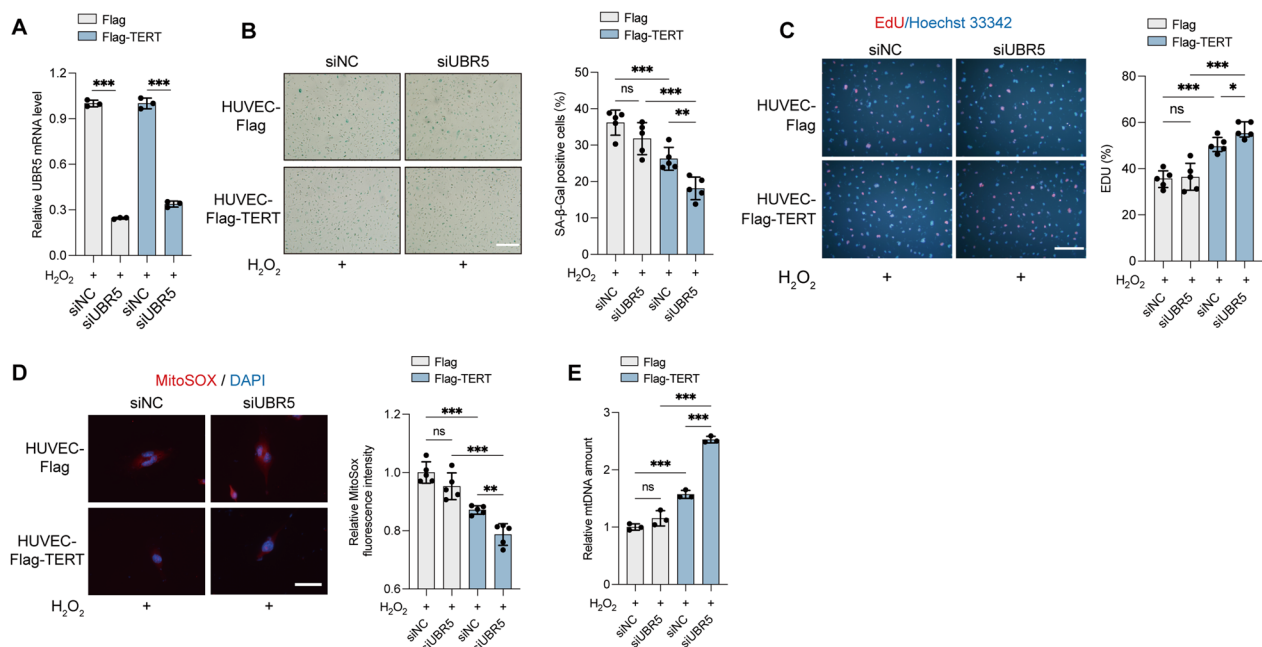
Fig. 6 Knockdown of UBR5 alleviates ROS production and senescence in HUVECs. **A–E** HUVEC-Flag and HUVEC-Flag-TERT cells were transiently transfected with siUBR5 or siNC and treated with 100 μM H_2O_2 for 6 h. **A** Relative UBR5 mRNA levels in HUVECs were measured by RT-qPCR. **B** Cells were subjected to SA-β-Gal staining; the percentage of SA-β-Gal-positive cells was quantified from five randomly selected fields. Scale bars, 500 μm. **C** EdU-labeled cells were stained with anti-EdU (red), and nuclei were counterstained with Hoechst 33342 (blue). The percentage of EdU-positive cells was quantified from five randomly selected fields. Scale bars, 150 μm. **D** Cells were stained with MitoSOX Red; nuclei were labeled with DAPI (blue). Scale bars, 30 μm. The relative MitoSOX fluorescence intensity was measured from five randomly selected fields. **E** Relative mtDNA content in cells was determined by RT-qPCR. (ns, not significant; *$P < 0.05$; **$P < 0.01$; ***$P < 0.001$)

other researchers have detected the presence of TERT in human microvascular endothelial cells as well as in HUVECs [56–58]. Our study indicated that sustained TERT expression was evident during the development of hiPSCs into VOs, but was downregulated once cells differentiated into a radially growing vascular network. In our model, the mRNA level of TERT and telomerase activity were not detected during the stages of vascular network formation and VOs. This may be due to the insufficient sensitivity of the TRAP assay or because TERT and telomerase activity are dramatically inhibited in our model system (occurring during the senescence of ECs). To explore TERT's protective role against oxidative stress, we treated VOs with H_2O_2 or oxLDL at the EPC stage. Our findings add to the evidence that telomerase has nonclassical functions, which are influenced by its subcellular localization and TERT levels. Notably, telomerase is involved in preventing apoptosis and maintaining redox homeostasis in somatic cells [59].

The overexpression of TERT counteracted the decrease in mtDNA content and the increase in mitochondrial ROS production, thus alleviating ROS-induced endothelial cell senescence. Beyer et al. first reported that telomerase's nontelomeric effects can influence vascular

physiology [58]. Specifically, in patients with coronary artery disease (CAD), decreased TERT protein levels in microvessels led to elevated mitochondrial ROS production due to reduced telomerase activity. TERT$^{-/-}$ rats treated with angiotensin II showed an increased myocardial infarction area after ischemia–reperfusion [12]. Interestingly, TERT has been localized to the mitochondria rather than the nucleus [58, 60], suggesting additional roles beyond telomere extension. Oxidative stress induces the nuclear export of TERT, a process dependent on the phosphorylation of TERT at Tyr707 by the Src kinase family [61]. Effective blood vessel function depends critically on normal cellular energy metabolism; thus, mitochondrial dysfunction and impaired energy metabolism can contribute to vascular aging and increased mitochondrial ROS release [1]. mtDNA, positioned near ROS production sites within mitochondria, lacks protective histone coverage and has limited repair mechanisms, resulting in a high mutation rate. These mutations and deletions exacerbate energy production disorders during cellular senescence [62]. Mitochondrial oxidative stress is implicated in vascular aging [2, 63], with mtDNA deletions identified in human atherosclerotic lesions [1]. Within the mitochondria, TERT

Zhao *et al. Journal of Translational Medicine*   (2024) 22:1080

Page 15 of 18

binds to mtDNA, protecting it from oxidative damage [15] and reducing the generation of mitochondrial ROS [64–66]. Overexpression of TERT decreases intracellular ROS production and enhances mitochondrial function [65–67].

After screening, we identified an interaction between the E3 ubiquitin ligase UBR5 and TERT. Intracellularly, UBR5, also known as E3 identified by differential display (EDD1), forms a complex with damage-specific DNA binding protein 1 (DDB1) and Vpr-binding protein (VPRBP), collectively known as the UBR5, DDB1, and VprBP (EDVP) complex [68]. UBR5, functioning as a HECT E3 ligase [42, 69, 70], recognizes specific substrates and ubiquitin chain topologies [71–73]. The EDVP complex acts as a scaffold protein for ubiquitinated TERT, and each component interacting with TERT in HeLa cells [42], consistent with our findings. Our results demonstrate that UBR5 negatively regulates TERT levels through ubiquitination. UBR5 contains two conserved domains: the HECT domain, which includes an N-lobe for E2 binding and a C-lobe [74] with a catalytically active cysteine that accepts ubiquitin from E2 to form the E3-ubiquitin complex [75, 76], and the PABC domain, involved in protein–protein interactions [77]. Our study highlights UBR5's crucial role in vascular oxidative stress-induced senescence. Inhibition of UBR5 alleviated oxidative stress-induced VO and endothelial cell senescence, as evidenced by reduced SA-β-Gal activity, increased EdU$^+$ cell count, decreased SASP factors secretion, maintenance of mitochondrial DNA content, and preserved redox homeostasis.

In summary, this study introduces a novel 3D VO model from hiPSCs and reveals a crucial interaction between the E3 ubiquitin ligase UBR5 and TERT. The identification of UBR5's role in negatively regulating TERT through ubiquitination provides novel insights into oxidative stress-induced senescence and offers potential avenues for targeted therapies against vascular damage. Despite the challenges posed by UBR5's large size and low expression of endogenous TERT, future advances in techniques like endogenous immunoprecipitation and purified protein studies are anticipated to address these issues and further clarify the UBR5-TERT interaction.

Innovation and value

- *Novel target identification*: We identified UBR5 as a significant regulator of TERT, which was not previously recognized in the context of vascular endothelial cells under oxidative stress. This novel finding provides new insights into the mechanisms controlling TERT stability and its protective effects.

- *Comprehensive models and methods*: Our study employed advanced models and techniques, including hiPSCs induced VOs, which offer a groundbreaking advantage as disease models by accurately replicating the intricate cellular, spatial, and molecular architecture of human vascular tissues, making them exceptionally valuable for studying complex vascular diseases.

- *Potential therapeutic implications*: By elucidating the role of UBR5 in TERT regulation and its impact on endothelial cell function, our research provides a new insight for therapeutic strategies aimed at enhancing vascular health and combating oxidative stress-related vascular diseases.

Conclusions
Our findings demonstrate that inhibiting UBR5 stabilizes TERT, which preserves EPC angiogenic capacity, reduces VO impairment, and delays endothelial cell senescence under oxidative stress. These findings highlight the potential of targeting UBR5 to enhance vascular health in oxidative stress-related conditions.

Abbreviations

VOs	Vascular organoids
CVD	Cardiovascular diseases
HUVECs	Human umbilical vein endothelial cells
ECs	Endothelial cells
hiPSCs	Human induced pluripotent stem cells
EPCs	Endothelial progenitor cells
TERT	Telomerase reverse transcriptase
UBR5	Ubiquitin protein ligase E3 component N-recognin 5
EDVP	UBR5, DDB1, and VprBP
PES1	Pescadillo ribosomal biogenesis factor 1
H_2O_2	Hydrogen peroxide
nLDL	Native low-density lipoprotein
oxLDL	Oxidized low-density lipoprotein
ROS	Reactive oxygen species
TRAP	Telomeric repeated amplification protocol
mtDNA	Mitochondrial DNA
SASP	Senescence-associated secretory phenotype
SA-β-Gal	Senescence-associated β-galactosidase
EdU	5-Ethynyl-2′-deoxyuridine
TNF	Tumor necrosis factor
IL6	Interleukin 6
IL8	Interleukin 8
CXCL1	C-X-C motif chemokine ligand 1
MMP1	Matrix metalloproteinase 1
LPS	Lipopolysaccharide
PDGFR-β	Platelet-derived growth factor receptor beta
Col IV	Collagen IV
α-SMA	Alpha-smooth muscle actin
CD31/PECAM-1	Platelet endothelial cell adhesion molecule-1
BMP4	Bone morphogenetic protein 4
FGF-2	Fibroblast growth factor 2
VEGF-A	Vascular endothelial growth factor A
p16^{INK4a}/CDKN2A	Cyclin dependent kinase inhibitor 2A
p21/CDKN1A	Cyclin dependent kinase inhibitor 1A
p53	Tumor protein p53
HSP70	Heat shock protein 70
HNRNPR	Heterogeneous nuclear ribonucleoprotein R
MAGED2	Melanoma-associated antigen D2

EDD1	E3 identified by differential display
DDB1	Damage-specific DNA binding protein 1
VPRBP	Vpr-binding protein

Supplementary Information

The online version contains supplementary material available at https://doi.org/10.1186/s12967-024-05887-0.

Supplementary Material 1.

Author contributions
All authors contributed to the study conception and design. Haijing Zhao, Nian Cao, and QiS Liu performed experiments, analyzed data, and wrote the first draft of the manuscript. Yingyue Zhang, Rui Jin, Huiying Lai, Li Zheng, Honghong Zhang, Yue Zhu, Yuhan Ma, Zengao Yang, Zhengfeng Wu, and Weini Li analyzed the data and discussed the results. Yundai Chen, Long Cheng, and Yuqi Liu designed the experiments and were responsible for the overall project concept.

Availability of data and materials
All data used in this study are available from the authors on reasonable request.

Declarations

Ethics approval and consent to participate
The manuscript does not contain clinical studies, patient data, or animal studies.

Consent for publication
Not applicable.

Competing interests
The authors have declared that no competing interest exists.

Author details
[1]Department of Cardiology, the Sixth Medical Centre, Chinese PLA General Hospital, Beijing 100037, People's Republic of China. [2]Medical School of Chinese PLA, Chinese PLA General Hospital, Beijing 100853, People's Republic of China. [3]The Key Laboratory of Geriatrics, Institute of Geriatric Medicine, Beijing Institute of Geriatrics, Chinese Academy of Medical Sciences, Beijing Hospital/National Centre of Gerontology of National Health Commission, Beijing 100730, People's Republic of China. [4]Beijing Institute of Biotechnology, Beijing 100850, People's Republic of China. [5]Department of Clinical Laboratory, Beijing Hospital, National Center of Gerontology, Institute of Geriatric Medicine, Chinese Academy of Medical Sciences, Beijing 100730, People's Republic of China. [6]School of Medicine, Nankai University, Tianjin 300071, People's Republic of China. [7]School of Medicine, South China University of Technology, Guangzhou 510006, People's Republic of China. [8]Department of Biomedical Science, Cedars-Sinai Cancer Institute, Cedars-Sinai Medical Center, Los Angeles, USA. [9]National Key Laboratory of Kidney Diseases, Beijing 100853, People's Republic of China. [10]Department of Cardiology, National Clinical Research Center of Geriatric Disease, Beijing 100853, People's Republic of China. [11]Beijing Key Laboratory of Chronic Heart Failure Precision Medicine, Beijing 100853, People's Republic of China.

References
1. Ungvari Z, Tarantini S, Donato AJ, Galvan V, Csiszar A. Mechanisms of vascular aging. Circ Res. 2018;123:849–67.
2. Csiszar A, Gautam T, Sosnowska D, Tarantini S, Banki E, Tucsek Z, Toth P, Losonczy G, Koller A, Reglodi D, et al. Caloric restriction confers persistent anti-oxidative, pro-angiogenic, and anti-inflammatory effects and promotes anti-aging miRNA expression profile in cerebromicrovascular endothelial cells of aged rats. Am J Physiol Heart Circ Physiol. 2014;307:H292-306.
3. Yan Q, Liu S, Sun Y, Chen C, Yang S, Lin M, Long J, Yao J, Lin Y, Yi F, et al. Targeting oxidative stress as a preventive and therapeutic approach for cardiovascular disease. J Transl Med. 2023;21:519.
4. Zinkevich NS, Gutterman DD. ROS-induced ROS release in vascular biology: redox-redox signaling. Am J Physiol Heart Circ Physiol. 2011;301:H647-653.
5. Zhao RZ, Jiang S, Zhang L, Yu ZB. Mitochondrial electron transport chain, ROS generation and uncoupling (review). Int J Mol Med. 2019;44:3–15.
6. Zhang Y, Murugesan P, Huang K, Cai H. NADPH oxidases and oxidase crosstalk in cardiovascular diseases: novel therapeutic targets. Nat Rev Cardiol. 2020;17:170–94.
7. Mu X, Liu SJ, Zheng LY, Ouyang C, Abdalla AME, Wang XX, Chen K, Yang FF, Meng N. The long coiled-coil protein NECC2 regulates oxLDL-induced endothelial oxidative damage and exacerbates atherosclerosis development in apolipoprotein E (-/-) mice. Free Radic Biol Med. 2024;216:106–17.
8. Khatana C, Saini NK, Chakrabarti S, Saini V, Sharma A, Saini RV, Saini AK. Mechanistic insights into the oxidized low-density lipoprotein-induced atherosclerosis. Oxid Med Cell Longev. 2020;2020:5245308.
9. Trpkovic A, Resanovic I, Stanimirovic J, Radak D, Mousa SA, Cenic-Milosevic D, Jevremovic D, Isenovic ER. Oxidized low-density lipoprotein as a biomarker of cardiovascular diseases. Crit Rev Clin Lab Sci. 2015;52:70–85.
10. Zhou H, Khan D, Hussain SM, Gerdes N, Hagenbeck C, Rana M, Cornelius JF, Muhammad S. Colchicine prevents oxidative stress-induced endothelial cell senescence via blocking NF-κB and MAPKs: implications in vascular diseases. J Inflamm (Lond). 2023;20:41.
11. de Lange T. Shelterin-mediated telomere protection. Annu Rev Genet. 2018;52:223–47.
12. Ait-Aissa K, Heisner JS, Norwood Toro LE, Bruemmer D, Doyon G, Harmann L, Geurts A, Camara AKS, Beyer AM. Telomerase deficiency predisposes to heart failure and ischemia-reperfusion injury. Front Cardiovasc Med. 2019;6:31.
13. Ale-Agha N, Jakobs P, Goy C, Zurek M, Rosen J, Dyballa-Rukes N, Metzger S, Greulich J, von Ameln F, Eckermann O, et al. Mitochondrial telomerase reverse transcriptase protects from myocardial ischemia/reperfusion injury by improving complex I composition and function. Circulation. 2021;144:1876–90.
14. Wang X, Guo Y, Cui T, Zhang T, Hu W, Liu R, Yin C. Telomerase reverse transcriptase restores pancreatic microcirculation profiles and attenuates endothelial dysfunction by inhibiting mitochondrial superoxide production: a potential target for acute pancreatitis therapy. Biomed Pharmacother. 2023;167: 115576.
15. Haendeler J, Dröse S, Büchner N, Jakob S, Altschmied J, Goy C, Spyridopoulos I, Zeiher AM, Brandt U, Dimmeler S. Mitochondrial telomerase reverse transcriptase binds to and protects mitochondrial DNA and function from damage. Arterioscler Thromb Vasc Biol. 2009;29:929–35.
16. Nitta E, Yamashita M, Hosokawa K, Xian M, Takubo K, Arai F, Nakada S, Suda T. Telomerase reverse transcriptase protects ATM-deficient hematopoietic stem cells from ROS-induced apoptosis through a telomere-independent mechanism. Blood. 2011;117:4169–80.
17. Miwa S, Czapiewski R, Wan T, Bell A, Hill KN, von Zglinicki T, Saretzki G. Decreased mTOR signalling reduces mitochondrial ROS in brain via accumulation of the telomerase protein TERT within mitochondria. Aging (Albany NY). 2016;8:2551–67.

Zhao *et al. Journal of Translational Medicine*   (2024) 22:1080

Page 17 of 18

18. Huang H, Huang W. Regulation of endothelial progenitor cell functions in ischemic heart disease: new therapeutic targets for cardiac remodeling and repair. Front Cardiovasc Med. 2022;9: 896782.

19. Martín-Bórnez M, Falcón D, Morrugares R, Siegfried G, Khatib AM, Rosado JA, Galeano-Otero I, Smani T. New insights into the reparative angiogenesis after myocardial infarction. Int J Mol Sci. 2023. https://doi.org/10.3390/ijms241512298.

20. Asahara T, Kawamoto A, Masuda H. Concise review: circulating endothelial progenitor cells for vascular medicine. Stem Cells. 2011;29:1650–5.

21. Peng J, Liu B, Ma QL, Luo XJ. Dysfunctional endothelial progenitor cells in cardiovascular diseases: role of NADPH oxidase. J Cardiovasc Pharmacol. 2015;65:80–7.

22. Wimmer RA, Leopoldi A, Aichinger M, Kerjaschki D, Penninger JM. Generation of blood vessel organoids from human pluripotent stem cells. Nat Protoc. 2019;14:3082–100.

23. Wimmer RA, Leopoldi A, Aichinger M, Wick N, Hantusch B, Novatchkova M, Taubenschmid J, Hämmerle M, Esk C, Bagley JA, et al. Human blood vessel organoids as a model of diabetic vasculopathy. Nature. 2019;565:505–10.

24. Clevers H. Modeling development and disease with organoids. Cell. 2016;165:1586–97.

25. Monteil V, Kwon H, Prado P, Hagelkrüys A, Wimmer RA, Stahl M, Leopoldi A, Garreta E, Hurtado Del Pozo C, Prosper F, et al. Inhibition of SARS-CoV-2 infections in engineered human tissues using clinical-grade soluble human ACE2. Cell. 2020;181:905-913.e907.

26. Jin R, Niu C, Wu F, Zhou S, Han T, Zhang Z, Li E, Zhang X, Xu S, Wang J, et al. DNA damage contributes to age-associated differences in SARS-CoV-2 infection. Aging Cell. 2022;21: e13729.

27. Cheng L, Yuan B, Ying S, Niu C, Mai H, Guan X, Yang X, Teng Y, Lin J, Huang J, et al. PES1 is a critical component of telomerase assembly and regulates cellular senescence. Sci Adv. 2019;5:eaav1090.

28. Harley J, Santosa MM, Ng CY, Grinchuk OV, Hor JH, Liang Y, Lim VJ, Tee WW, Ong DST, Ng SY. Telomere shortening induces aging-associated phenotypes in hiPSC-derived neurons and astrocytes. Biogerontology. 2024;25:341–60.

29. Polonio AM, Medrano M, Chico-Sordo L, Córdova-Oriz I, Cozzolino M, Montans J, Herraiz S, Seli E, Pellicer A, García-Velasco JA, Varela E. Impaired telomere pathway and fertility in senescence-accelerated mice prone 8 females with reproductive senescence. Aging (Albany NY). 2023;15:4600–24.

30. Chatterjee S, Leach-Mehrwald M, Huang CK, Xiao K, Fuchs M, Otto M, Lu D, Dang V, Winkler T, Dunbar CE, et al. Telomerase is essential for cardiac differentiation and sustained metabolism of human cardiomyocytes. Cell Mol Life Sci. 2024;81:196.

31. Xing J, Chen M, Wood CG, Lin J, Spitz MR, Ma J, Amos CI, Shields PG, Benowitz NL, Gu J, et al. Mitochondrial DNA content: its genetic heritability and association with renal cell carcinoma. J Natl Cancer Inst. 2008;100:1104–12.

32. Kaaman M, Sparks LM, van Harmelen V, Smith SR, Sjölin E, Dahlman I, Arner P. Strong association between mitochondrial DNA copy number and lipogenesis in human white adipose tissue. Diabetologia. 2007;50:2526–33.

33. Shu L, Hu C, Xu M, Yu J, He H, Lin J, Sha H, Lu B, Engelender S, Guan M, Song Z. ATAD3B is a mitophagy receptor mediating clearance of oxidative stress-induced damaged mitochondrial DNA. Embo j. 2021;40: e106283.

34. Hunter SE, Jung D, Di Giulio RT, Meyer JN. The QPCR assay for analysis of mitochondrial DNA damage, repair, and relative copy number. Methods. 2010;51:444–51.

35. Nikolova MT, He Z, Wimmer RA, Seimiya M, Nikoloff JM, Penninger JM, Camp JG, Treutlein B. Fate and state transitions during human bloodvessel organoid development. bioRxiv. 2022;10:2036.

36. Everaert BR, Van Craenenbroeck EM, Hoymans VY, Haine SE, Van Nassauw L, Conraads VM, Timmermans JP, Vrints CJ. Current perspective of pathophysiological and interventional effects on endothelial progenitor cell biology: focus on PI3K/AKT/eNOS pathway. Int J Cardiol. 2010;144:350–66.

37. Kattoor AJ, Pothineni NVK, Palagiri D, Mehta JL. Oxidative stress in atherosclerosis. Curr Atheroscler Rep. 2017;19:42.

38. Takahashi A, Ohtani N, Hara E. Irreversibility of cellular senescence: dual roles of p16INK4a/Rb-pathway in cell cycle control. Cell Div. 2007;2:10.

39. Shokolenko I, Venediktova N, Bochkareva A, Wilson GL, Alexeyev MF. Oxidative stress induces degradation of mitochondrial DNA. Nucleic Acids Res. 2009;37:2539–48.

40. Liu R, Cheng F, Zeng K, Li W, Lan J. GPR120 agonist GW9508 ameliorated cellular senescence induced by ox-LDL. ACS Omega. 2020;5:32195–202.

41. Liu R, Liu H, Ha Y, Tilton RG, Zhang W. Oxidative stress induces endothelial cell senescence via downregulation of Sirt6. Biomed Res Int. 2014;2014: 902842.

42. Jung HY, Wang X, Jun S, Park JI. Dyrk2-associated EDD-DDB1-VprBP E3 ligase inhibits telomerase by TERT degradation. J Biol Chem. 2013;288:7252–62.

43. Venteicher AS, Meng Z, Mason PJ, Veenstra TD, Artandi SE. Identification of ATPases pontin and reptin as telomerase components essential for holoenzyme assembly. Cell. 2008;132:945–57.

44. Huang J, Wang F, Okuka M, Liu N, Ji G, Ye X, Zuo B, Li M, Liang P, Ge WW, et al. Association of telomere length with authentic pluripotency of ES/iPS cells. Cell Res. 2011;21:779–92.

45. Teichroeb JH, Kim J, Betts DH. The role of telomeres and telomerase reverse transcriptase isoforms in pluripotency induction and maintenance. RNA Biol. 2016;13:707–19.

46. Orlova VV, van den Hil FE, Petrus-Reurer S, Drabsch Y, Ten Dijke P, Mummery CL. Generation, expansion and functional analysis of endothelial cells and pericytes derived from human pluripotent stem cells. Nat Protoc. 2014;9:1514–31.

47. Orlova VV, Drabsch Y, Freund C, Petrus-Reurer S, van den Hil FE, Muenthaisong S, Dijke PT, Mummery CL. Functionality of endothelial cells and pericytes from human pluripotent stem cells demonstrated in cultured vascular plexus and zebrafish xenografts. Arterioscler Thromb Vasc Biol. 2014;34:177–86.

48. Yu J. Vascularized organoids: a more complete model. Int J Stem Cells. 2021;14:127–37.

49. Romeo SG, Secco I, Schneider E, Reumiller CM, Santos CXC, Zoccarato A, Musale V, Pooni A, Yin X, Theofilatos K, et al. Human blood vessel organoids reveal a critical role for CTGF in maintaining microvascular integrity. Nat Commun. 2023;14:5552.

50. Thum T, Fraccarollo D, Galuppo P, Tsikas D, Frantz S, Ertl G, Bauersachs J. Bone marrow molecular alterations after myocardial infarction: impact on endothelial progenitor cells. Cardiovasc Res. 2006;70:50–60.

51. Turgeon J, Haddad P, Dussault S, Groleau J, Maingrette F, Perez G, Rivard A. Protection against vascular aging in Nox2-deficient mice: impact on endothelial progenitor cells and reparative neovascularization. Atherosclerosis. 2012;223:122–9.

52. Yuan X, Xu D. Telomerase reverse transcriptase (TERT) in action: crosstalking with epigenetics. Int J Mol Sci. 2019;20:3338.

53. Takano H, Murasawa S, Asahara T. Functional and gene expression analysis of hTERT overexpressed endothelial cells. Biologics. 2008;2:547–54.

54. Greenberg RA, Allsopp RC, Chin L, Morin GB, DePinho RA. Expression of mouse telomerase reverse transcriptase during development, differentiation and proliferation. Oncogene. 1998;16:1723–30.

55. Bär C, Bernardes de Jesus B, Serrano R, Tejera A, Ayuso E, Jimenez V, Formentini I, Bobadilla M, Mizrahi J, de Martino A, et al. Telomerase expression confers cardioprotection in the adult mouse heart after acute myocardial infarction. Nat Commun. 2014;5:5863.

56. Hughes WE, Chabowski DS, Ait-Aissa K, Fetterman JL, Hockenberry J, Beyer AM, Gutterman DD. Critical interaction between telomerase and autophagy in mediating flow-induced human arteriolar vasodilation. Arterioscler Thromb Vasc Biol. 2021;41:446–57.

57. Kurz DJ, Hong Y, Trivier E, Huang HL, Decary S, Zang GH, Lüscher TF, Erusalimsky JD. Fibroblast growth factor-2, but not vascular endothelial growth factor, upregulates telomerase activity in human endothelial cells. Arterioscler Thromb Vasc Biol. 2003;23:748–54.

58. Beyer AM, Freed JK, Durand MJ, Riedel M, Ait-Aissa K, Green P, Hockenberry JC, Morgan RG, Donato AJ, Peleg R, et al. Critical role for telomerase in the mechanism of flow-mediated dilation in the human microcirculation. Circ Res. 2016;118:856–66.

59. Rosen J, Jakobs P, Ale-Agha N, Altschmied J, Haendeler J. Non-canonical functions of telomerase reverse transcriptase—impact on redox homeostasis. Redox Biol. 2020;34: 101543.

60. Durand MJ, Zinkevich NS, Riedel M, Gutterman DD, Nasci VL, Salato VK, Hijjawi JB, Reuben CF, North PE, Beyer AM. Vascular actions of angiotensin

Zhao *et al. Journal of Translational Medicine*   (2024) 22:1080

Page 18 of 18

1–7 in the human microcirculation: novel role for telomerase. Arterioscler Thromb Vasc Biol. 2016;36:1254–62.

61. Haendeler J, Hoffmann J, Brandes RP, Zeiher AM, Dimmeler S. Hydrogen peroxide triggers nuclear export of telomerase reverse transcriptase via Src kinase family-dependent phosphorylation of tyrosine 707. Mol Cell Biol. 2003;23:4598–610.

62. Wenzel P, Schuhmacher S, Kienhofer J, Muller J, Hortmann M, Oelze M, Schulz E, Treiber N, Kawamoto T, Scharffetter-Kochanek K, et al. Manganese superoxide dismutase and aldehyde dehydrogenase deficiency increase mitochondrial oxidative stress and aggravate age-dependent vascular dysfunction. Cardiovasc Res. 2008;80:280–9.

63. Springo Z, Tarantini S, Toth P, Tucsek Z, Koller A, Sonntag WE, Csiszar A, Ungvari Z. Aging exacerbates pressure-induced mitochondrial oxidative stress in mouse cerebral arteries. J Gerontol A Biol Sci Med Sci. 2015;70:1355–9.

64. Green PD, Sharma NK, Santos JH. Telomerase impinges on the cellular response to oxidative stress through mitochondrial ROS-mediated regulation of autophagy. Int J Mol Sci. 2019;20:1509.

65. Ahmed S, Passos JF, Birket MJ, Beckmann T, Brings S, Peters H, Birch-Machin MA, von Zglinicki T, Saretzki G. Telomerase does not counteract telomere shortening but protects mitochondrial function under oxidative stress. J Cell Sci. 2008;121:1046–53.

66. Singhapol C, Pal D, Czapiewski R, Porika M, Nelson G, Saretzki GC. Mitochondrial telomerase protects cancer cells from nuclear DNA damage and apoptosis. PLoS ONE. 2013;8: e52989.

67. Indran IR, Hande MP, Pervaiz S. hTERT overexpression alleviates intracellular ROS production, improves mitochondrial function, and inhibits ROS-mediated apoptosis in cancer cells. Cancer Res. 2011;71:266–76.

68. Maddika S, Chen J. Protein kinase DYRK2 is a scaffold that facilitates assembly of an E3 ligase. Nat Cell Biol. 2009;11:409–19.

69. Shah SS, Kumar S. Adaptors as the regulators of HECT ubiquitin ligases. Cell Death Differ. 2021;28:455–72.

70. Cho JH, Kim SA, Seo YS, Park SG, Park BC, Kim JH, Kim S. The p90 ribosomal S6 kinase-UBR5 pathway controls Toll-like receptor signaling via miRNA-induced translational inhibition of tumor necrosis factor receptor-associated factor 3. J Biol Chem. 2017;292:11804–14.

71. Shearer RF, Iconomou M, Watts CK, Saunders DN. Functional roles of the E3 ubiquitin ligase UBR5 in cancer. Mol Cancer Res. 2015;13:1523–32.

72. Kokeny G, Calvier L, Legchenko E, Chouvarine P, Mozes MM, Hansmann G. PPARgamma is a gatekeeper for extracellular matrix and vascular cell homeostasis: beneficial role in pulmonary hypertension and renal/cardiac/pulmonary fibrosis. Curr Opin Nephrol Hypertens. 2020;29:171–9.

73. Pan Z, Li GF, Sun ML, Xie L, Liu D, Zhang Q, Yang XX, Xia S, Liu X, Zhou H, et al. MicroRNA-1224 splicing circularRNA-Filip1l in an Ago2-dependent manner regulates chronic inflammatory pain via targeting Ubr5. J Neurosci. 2019;39:2125–43.

74. Qian H, Zhang Y, Wu B, Wu S, You S, Zhang N, Sun Y. Structure and function of HECT E3 ubiquitin ligases and their role in oxidative stress. J Transl Int Med. 2020;8:71–9.

75. Jiang W, Wang S, Xiao M, Lin Y, Zhou L, Lei Q, Xiong Y, Guan KL, Zhao S. Acetylation regulates gluconeogenesis by promoting PEPCK1 degradation via recruiting the UBR5 ubiquitin ligase. Mol Cell. 2011;43:33–44.

76. Li CG, Mahon C, Sweeney NM, Verschueren E, Kantamani V, Li D, Hennigs JK, Marciano DP, Diebold I, Abu-Halawa O, et al. PPARgamma interaction with UBR5/ATMIN promotes DNA repair to maintain endothelial homeostasis. Cell Rep. 2019;26(1333–1343): e1337.

77. Feng H, Lu J, Song X, Thongkum A, Zhang F, Lou L, Reizes O, Almasan A, Gong Z. CK2 kinase-mediated PHF8 phosphorylation controls TopBP1 stability to regulate DNA replication. Nucleic Acids Res. 2020;48:10940–52.

Publisher's Note